Supplementary Material

Lithium halide filled carbon nanocapsules: paving the way towards lithium neutron capture therapy (LiNCT)

Gil Gonçalves[a,b], Stefania Sandoval[a], Marina Llenas[a], Belén Ballesteros[c], Tatiana Da Ros[d], Silva Bortolussi[e,f], Laura Cansolino[f,g], Cinzia Ferrarie[g], Ian Postuma[f], Nicoletta Protti[e,f], Manuel Melle-Franco[h], Saverio Altieri[e,f], Gerard Tobías-Rossell[a]**

[a] Institut de Ciència de Materials de Barcelona (ICMAB-CSIC) Campus de la UAB, 08193, Bellaterra, Spain

[b] TEMA, Mechanical Engineering Department, University of Aveiro, 3810-193 Aveiro, Portugal

[c] Catalan Institute of Nanoscience and Nanotechnology (ICN2), CSIC and The Barcelona Institute of Science and Technology, Campus UAB, Bellaterra, 08193, Barcelona, Spain

[d] INSTM - Trieste unit - Department of Chemical and Pharmaceutical Sciences, University of Trieste, Via L. Giorgieri 1, 34127, Trieste, Italy

[e] University of Pavia, Department of Physics, Pavia, Italy

[f] Istituto Nazionale di Fisica Nucleare (INFN), the Unit of Pavia, Pavia, Italy

[g] University of Pavia, Department of Clinic-Surgical Sciences, Experimental Surgery Laboratory, Pavia, Italy

[h] CICECO−Aveiro Institute of Materials, Department of Chemistry, University of Aveiro, 3810-193 Aveiro, Portugal

1. Particle size distribution and morphological analysis of MWCNTs and CNHs

The final length distribution of the acid treated/centrifuged MWCNTs was calculated based on scanning electron microscopy (SEM) images. Figure S1 a) and b) show representative SEM images of MWCNTs centrifuged at different speeds. Statistical analyses reveal an average length distribution of 186.2 ± 81.9 nm and 144.3 ± 53.9 nm after centrifugation at 4000 and 20000 rpm, respectively.

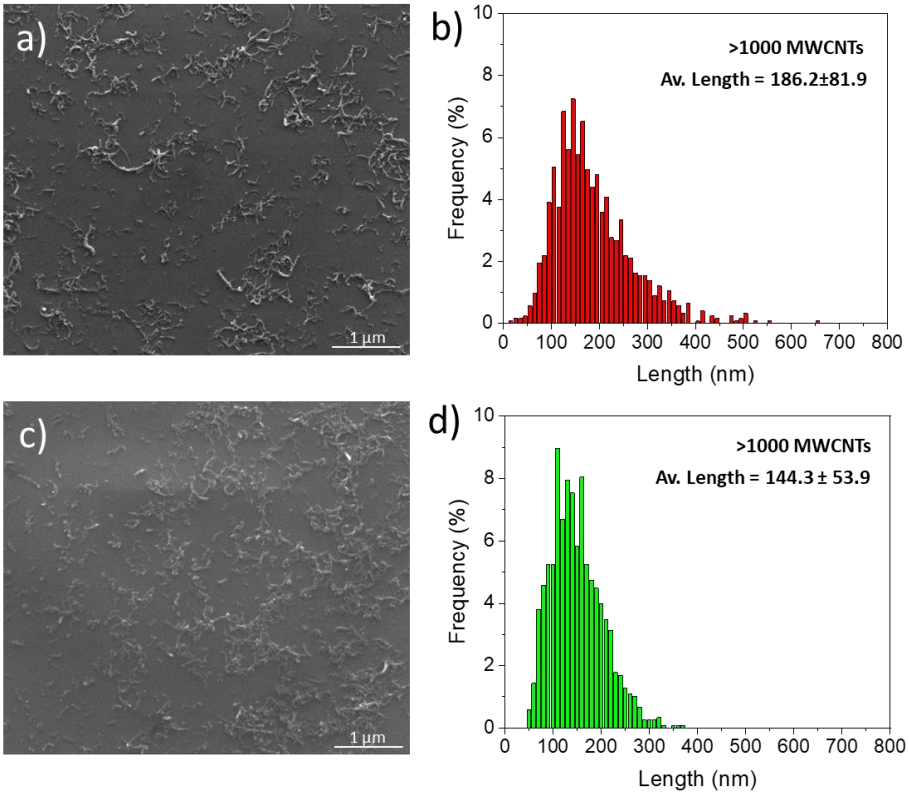

Figure S1. SEM images of MWCNTs after the employed acid treatment followed by centrifugation at 4000 rpm a) and c) 20000 rpm, b) and d) show the respective length distribution histograms obtained by measuring over 1000 individual MWCNTs.

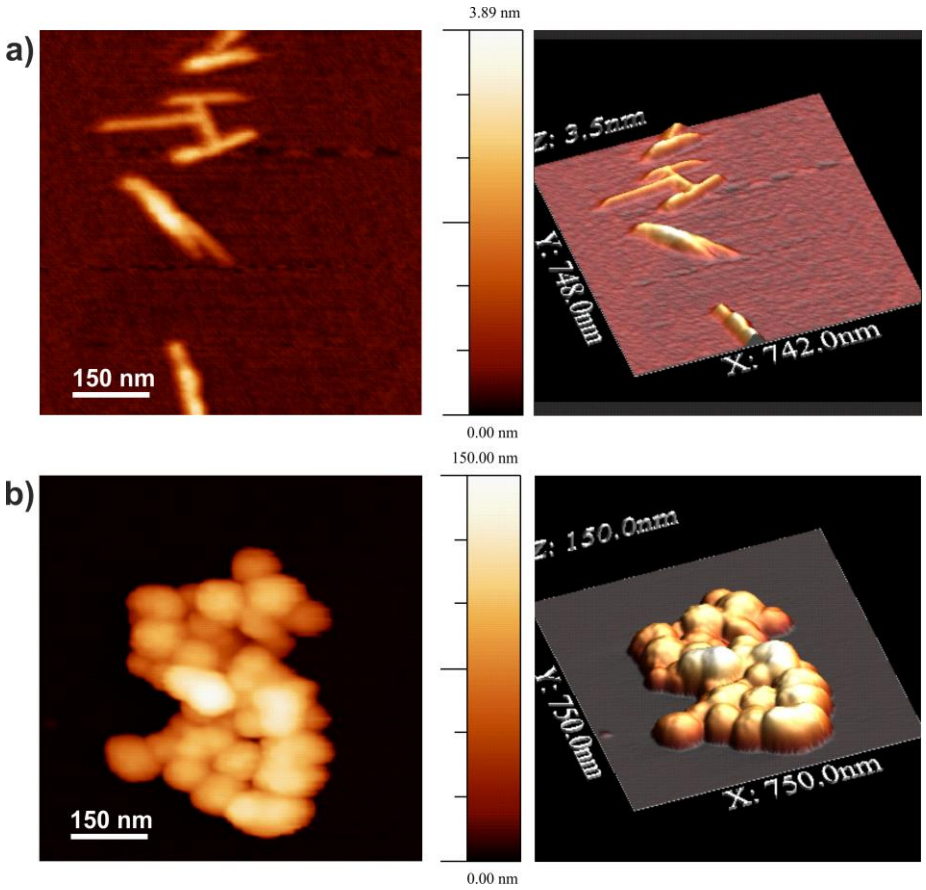

Figure S2. AFM images of acid treated and centrifuged a) MWCNTs (20000 rpm) and b) CNHs after the oxidizing treatment (500 ºC).

2. Thermogravimetric analysis of MWCNTs

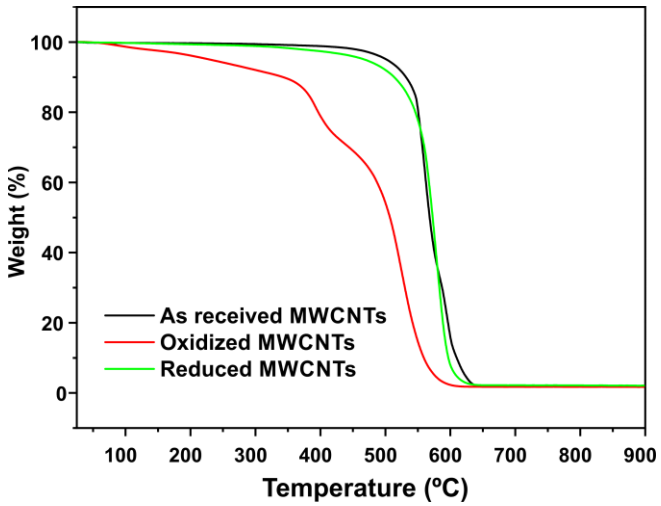

Figure S3. Thermogravimetry analysis under flowing air of as-received MWCNTs (black line), after oxidizing acid/centrifuge treatment (red line) and after the reduction treatment under vacuum at 800 °C during 2 h (green line).

3. BET analysis of annealed CNHs

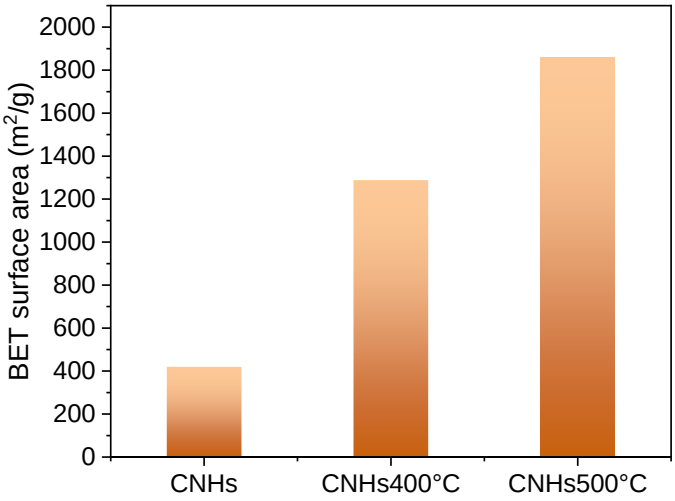

Figure S4. Specific surface area determined by BET analysis for as received carbon nanohorns (CNHs) and CNHs thermally treated in air at a heating rate of 1 °C·min^{-1} up to 400 °C (CNHs400°C) or 500 °C (CNHs500°C).

4. Thermogravimetric analysis of CNHs

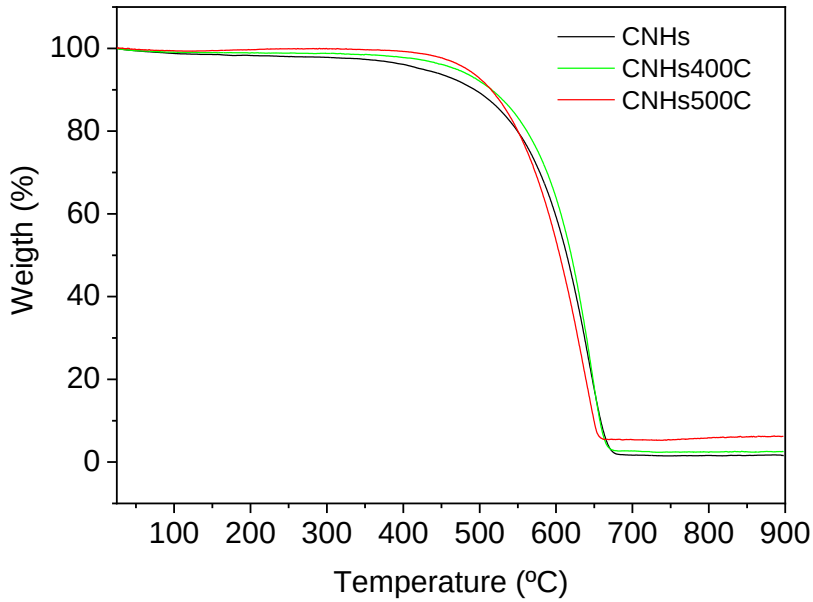

Figure S5. Thermogravimetry analysis under flowing air of as-received CNHs (black line), and thermally treated at 400 °C (green line) and 500 °C (red line).

5. Size distribution analysis of carbon nanohorns

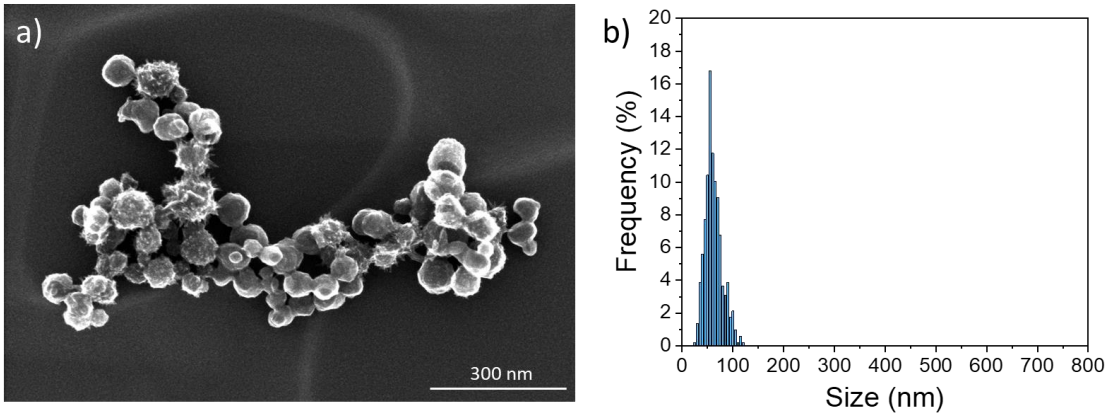

Figure S6. a) SEM image of CNHs after the oxidizing treatment (500 ºC), and b) size distribution histograms obtained by measuring over 500 individual CNHs.

6. Reactional mixture encapsulated in silica ampule after thermal treatment

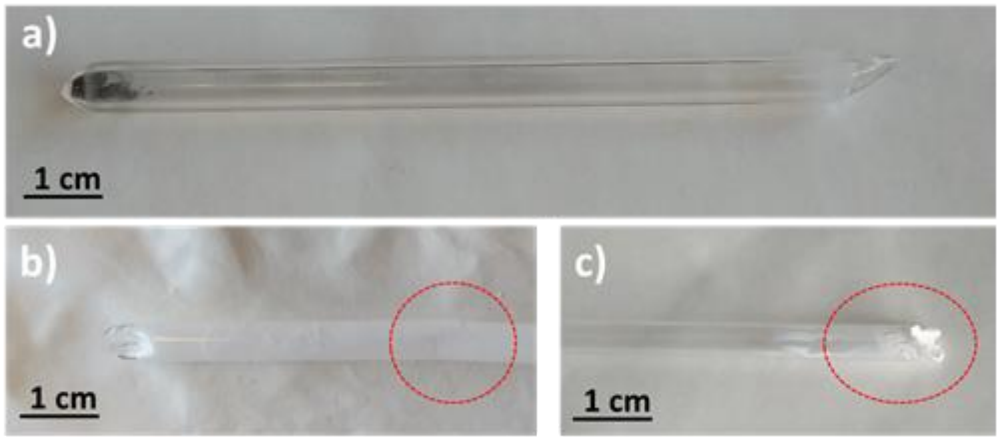

Figure S7. A mixture of lithium compound and short-MWCNTs sealed in a silica tube after the thermal treatment: **a)** LiI, **b)** LiF and **c)** LiCl. The red circles highlight the damage promoted by the different lithium compounds to the silica tube during the synthesis process.

7. HAADF STEM images of ^{6}LiI encapsulated into CNCs

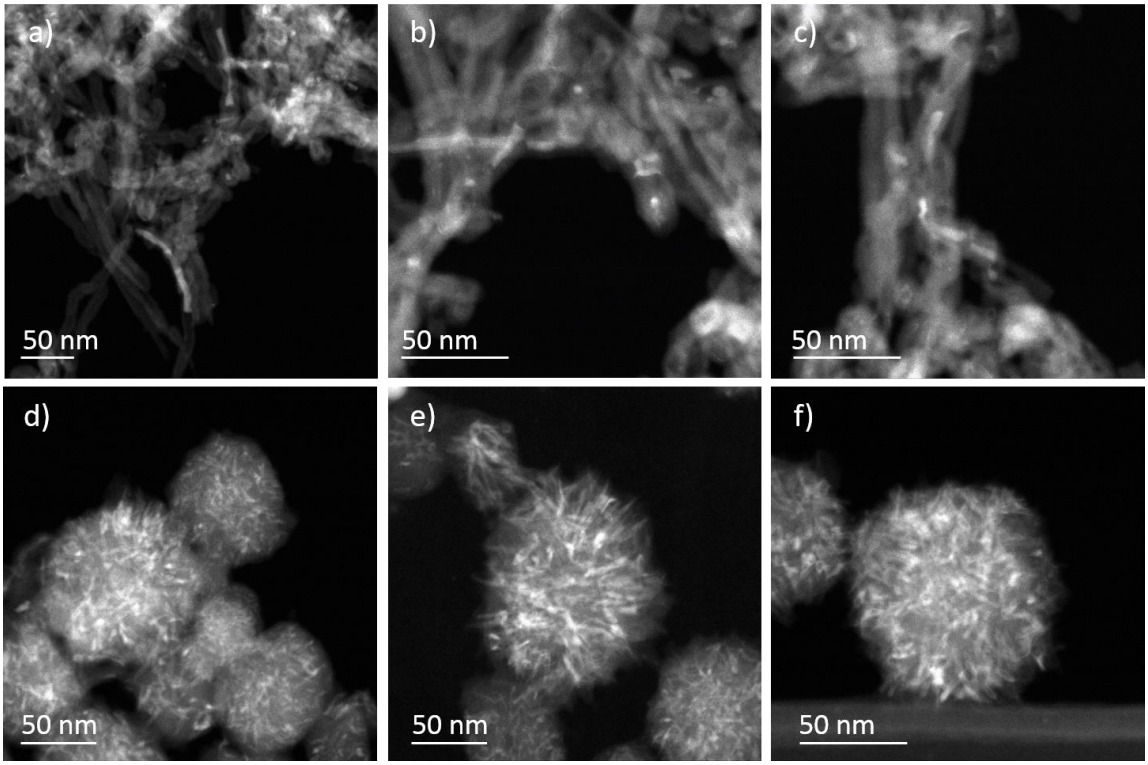

Figure S8. Additional HAADF STEM images of ^{6}LiI encapsulated into MWCNTs (a-c) and CNHs (d-f). In these Z-contrast images ^{6}LiI appears as bright lines following the internal cavities of the MWCNTs and CNHs, in agreement with the high intensity expected for I (Z=53) with respect to C (Z=6).

8. Energy dispersing X-ray (EDX)

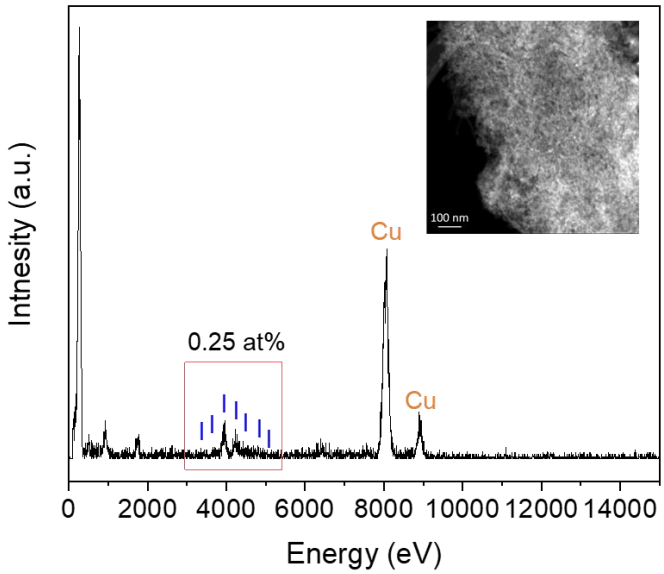

Figure S9. Energy Dispersive X-Ray analysis of ^{6}LiI@MWCNTs. The inset corresponds to the area of the sample where the data was acquired.

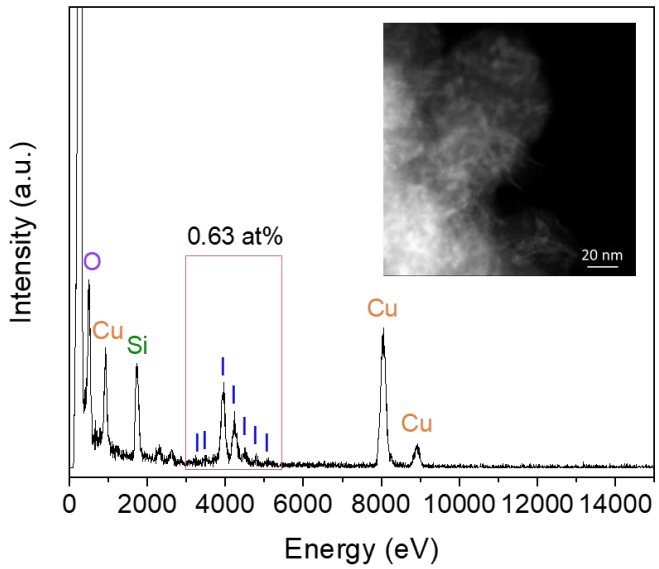

Figure S10. Energy Dispersive X-Ray analysis of the sample ^{6}LiI@CNHs. The inset corresponds to the area of the sample where the data was acquired.

9. XPS spectra of ^{6}LiI@CNCs.

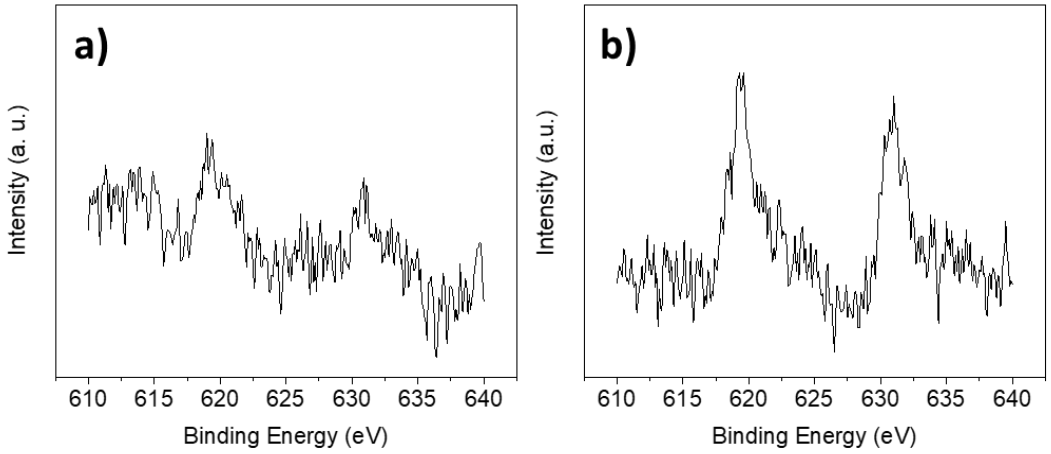

Figure S11. High resolution XPS spectrum of I3d for a) ^{6}LiI@MWCNTs and b) ^{6}LiI@CNHs samples.

10. HRTEM and HAADF STEM imaging of ^{6}LiI@MWCNTs and ^{6}LiI@CNHs

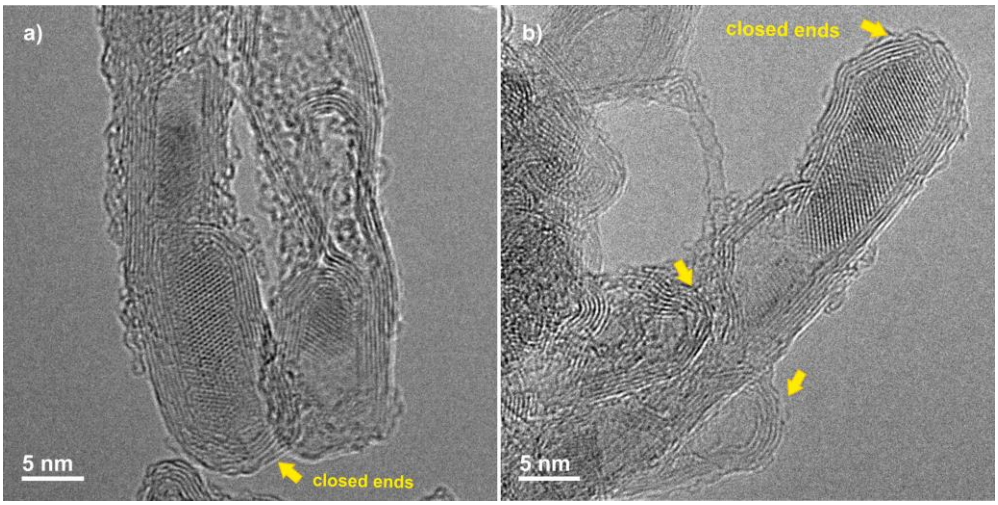

Figure S12. HRTEM images of ^{6}LiI encapsulated into MWCNTs. Annealing treatments lead to the simultaneous filling and end-closing of the carbon nanotubes (carbon nanocapsules).

11. Computer models of LiI@CNCs

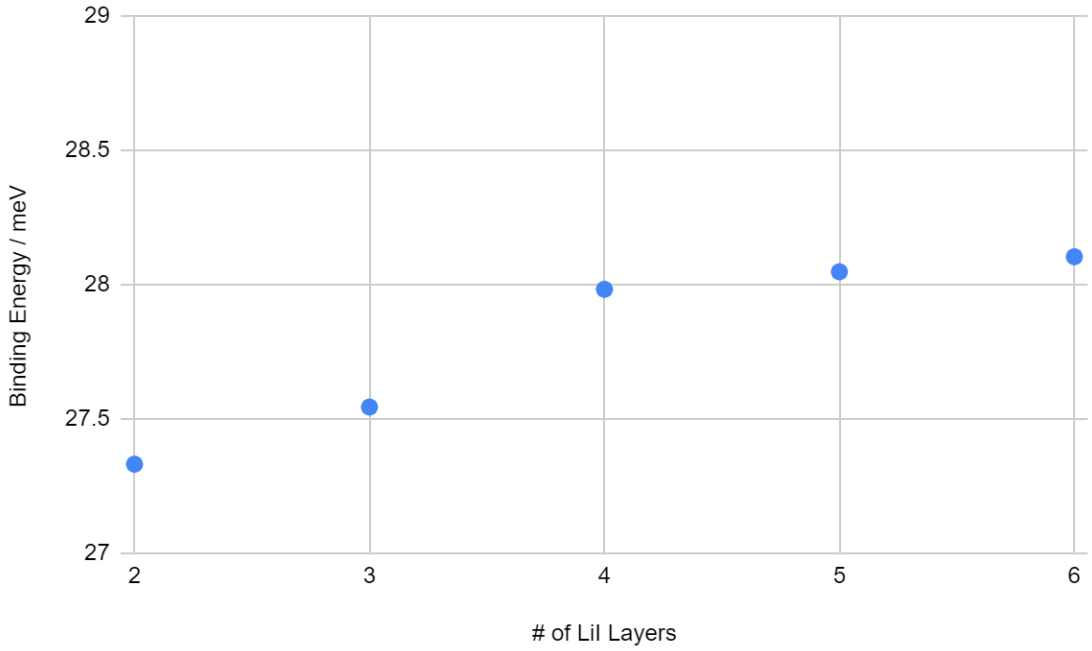

Figure S13. Binding energy per carbon atom for an increasing number of LiI (100) layers adsorbed on graphene.

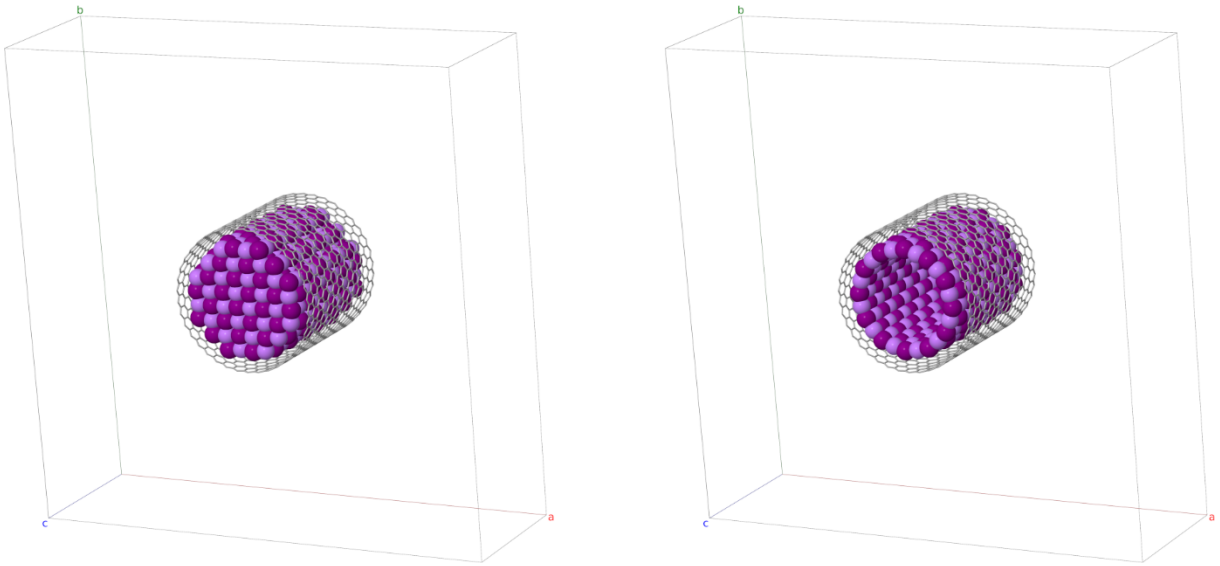

Figure S14. Periodic cells used to model LiI@CNTs.

12. Surface functionalization of carbon nanocapsules

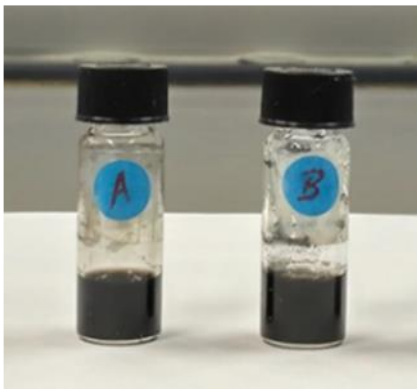

Figure S15. Water dispersion stability after 24 h of the NH_2_^{6}Li@CNCs with a concentration of 1 mg/mL of CNHs (A) and short-MWCNTs (B).

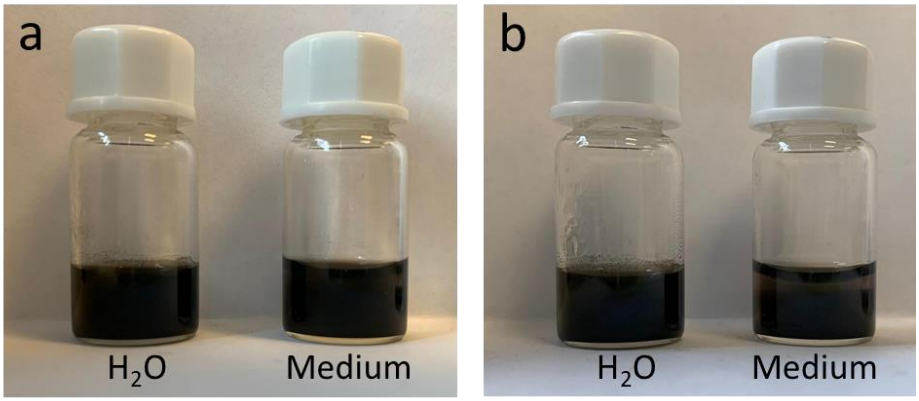

Figure S16. Dispersion stability of NH_2_^{6}Li@CNHs with a concentration of 1 mg/mL in water and cell culture medium a) after 24 h and b) after 7 days. After 7 days, a better dispersability is observed in water than in medium. Note that dispersion a) in water is a replica to that of Fig. S15-A.

13. Sample composition analyses

Table S1. Sample composition, considering the atomic ratio obtained from the high resolution C1s, N1s and I3d XPS for the carbon nanocapsules before (^{6}LiI@MWCNTs and ^{6}LiI@CNHs) and after surface functionalization by cycloaddition reaction (NH_2_^{6}LiI@MWCNTs and NH_2_^{6}LiI@CNHs). H* and Li** contents were determined based on the stoichiometry of both the aromatic moiety attached to the carbon surface (C_6NH_7) and the lithium iodide (1:1).

Sample	Element (at. %)				
	C	N	H*	I	Li**
^{6}LiI@MWCNT	97.2	/	/	1.4	1.4
^{6}LiI@CNH	93.0	/	/	3.5	3.5
NH_2_^{6}LiI@MWCNT	83.5	1.9	13.2	0.7	0.7
NH_2_^{6}LiI@CNH	82.9	1.9	13.2	1.0	1.0

14. Neutron autoradiography of cell samples treated with NH_2_^{6}LiI@CNCs

Figure S17 shows three samples of cells treated with MWCNT. The non-uniformity of lithium distribution is evident (in a, b and c) as the white spots are randomly scattered within the area of the sample. As a guide to the eye, the area of the sample has been contoured in yellow.

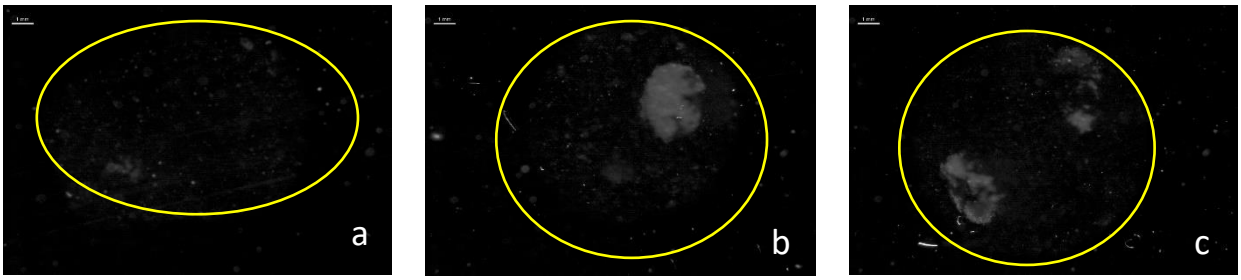

Figure S17. Neutron autoradiography of 3 cell samples treated with NH_2_^{6}LiI@MWCNT. The scale bar corresponds to 1 mm.

Figure S18 presents additional images of cells treated with CNH (d, e and f), showing a more uniform distribution of lithium, as the white structures are disseminated over the entire sample. This means that lithium was more available to the cells in the culture, and that a more

homogeneous uptake than with MWNT has occurred. As a guide to the eye, the area of the sample has been contoured in yellow.

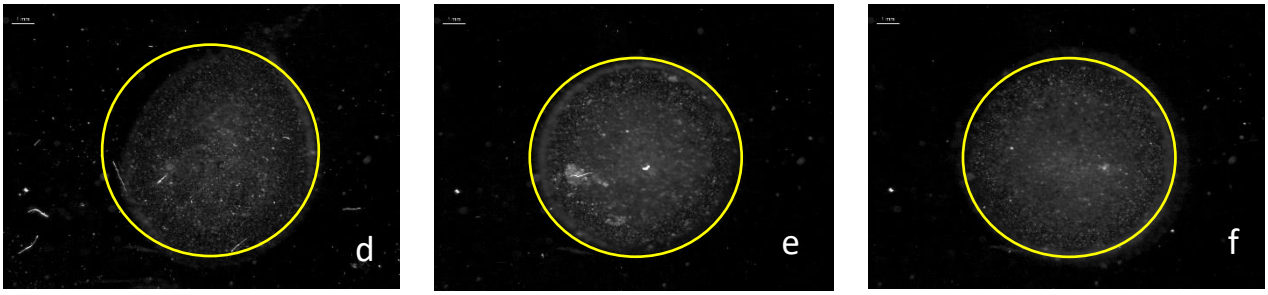

Figure S18. Neutron autoradiography of 3 cell samples treated with NH_2_^{6}LiI@CNH. The scale bar corresponds to 1 mm.